Atmos. Chem. Phys. Discuss., https://doi.org/10.5194/acp-2018-661
Manuscript under review for journal Atmos. Chem. Phys.
Discussion started: 24 July 2018
© Author(s) 2018. CC BY 4.0 License.

Spatial and temporal changes of SO_2 regimes over China in recent decade and the driving mechanism

Ting Wang[1], Pucai Wang[1, 3], Nicolas Theys[2], François Hendrick[2], Michel Van Roozendael[2]

1 CAS Key Laboratory of Middle Atmosphere and Global Environment Observation, Institute of Atmospheric Physics, Chinese Academy of Sciences, Beijing, China

2 Belgian Institute for Space Aeronomy (IASB-BIRA), Brussels, Belgium

3 University of Chinese Academy of Sciences, Beijing 100049, China

Correspondence to:

Ting Wang, Institute of Atmospheric Physics, Chinese Academy of Sciences, Beijing 100029, E-mail: wangting@mail.iap.ac.cn

© Author(s) 2018. CC BY 4.0 License.

Abstract: The spatial and temporal changes of SO_2 regimes over China during 2005 to 2016 and their associated driving mechanism are investigated based on a state-of-the-art retrieval dataset. Climatological SO_2 exhibits pronounced seasonal and regional variations, with higher loadings in wintertime and two prominent maxima centered in the North China Plain and the Cheng-Yu District. In the last decade, overall SO_2 decreasing trends have been reported nationwide, with spatially varying downward rates according to a general rule—the higher the SO_2 loading, the more significant the decrease. However, such decline is in fact not monotonic, but instead four distinct temporal regimes can be identified by empirical orthogonal function analysis. After an initial rise at the beginning, SO_2 in China undergoes two sharp drops in the periods 2007-2008 and 2014-2016, amid which 5-year moderate rebounding or stagnation is sustained. Despite spatial coherent behaviors, different mechanisms are tied to North China and South China, delimited roughly by the Yangtze River. In North China, the same four regimes are detected in the time series of emission that is expected to drive the regime of atmospheric SO_2, with a percentage of explained variance amounting to 81%. Out of total emission, those from industrial sector dominate SO_2 variation throughout the whole period, while household emission fluctuates little until 2008 but afterwards acts to partially offset the effect caused by industrial emission. In contrast to North China, SO_2 emissions in South China exhibit a continuous descending tendency, due to the gradual cuts of industrial emissions together with a sudden downward shift of household emissions. As a result, the role of emissions only makes up about one third

© Author(s) 2018. CC BY 4.0 License.

of the SO_2 variation, primarily owing to the decoupled pathways of emission and atmospheric content during 2009 to 2013 when the emissions continue to decline but atmospheric content witnesses a rebound. Unfavorable meteorological conditions, including deficient precipitation, weaker wind speed and increased static stability, outweigh the effect of decreasing emissions and thus give rise to the rebound of SO_2 during 2009 to 2013.

Key words: SO_2, China, spatiotemporal regimes, mechanism

Atmos. Chem. Phys. Discuss., https://doi.org/10.5194/acp-2018-661
Manuscript under review for journal Atmos. Chem. Phys.
Discussion started: 24 July 2018
© Author(s) 2018. CC BY 4.0 License.

1 Introduction

In recent decade, air pollution has persistently plagued China, especially in leading economic and densely populated areas (Chan and Yao 2008; Ma et al., 2012; Chai et al., 2014). In China, environmental protection agencies identify six major pollutants of concern, including sulfur dioxide (SO_2), nitrogen dioxide (NO_2), ozone (O_3), carbon monoxide (CO), fine particulate matter (PM2.5) and coarse particulate matter (PM10). Then, values of the six pollutants are transformed into a single number called Air Quality Index (AQI) for effective communication of air quality status and corresponding health impact (MEPC, 2012).

SO_2 is one of the six major pollutants in China (Ren et al., 2017). It is harmful to human health, affecting lung function, worsening asthma attacks and aggravating existing heart disease (WHO, 2018). It also leads to the acidification of the atmosphere, and the formed sulfate aerosol is one of the most important components of fine particles in cities (Meng et al., 2009). Overall, SO_2 is a key influencing factor for atmospheric pollution, and it poses great threats to life, property and environment (Wang et al., 2014).

Compared to airborne and ground-based remote sensing, satellite platforms permit near-global coverage on a continuing and repetitive basis, enabling quick and large-scale estimation of pollution patterns (Yu et al., 2010). Since the world's first weather satellite TIROS-I launched in 1960, satellites have become a crucial part of Earth's observations and practical applications (Yu et al., 2010). Till now, SO_2 has been measured globally by several operational satellite instruments, such as OMPS (Zhang

© Author(s) 2018. CC BY 4.0 License.

et al., 2017), GOME-2 (Munro et al., 2006; Rix et al., 2010) and OMI (Lee et al., 2011; Li et al., 2013; Theys et al., 2015).

With the aid of satellite data, in the past decade, various attempts have been made to explore the variation of SO_2 loadings in China. Lu et al. (2010) report that total SO_2 emissions in China have increased by 53% from 2000 to 2006, followed by a growth rate slowdown and the start of a decrease. Li et al. (2010), Yan et al. (2014), and Zhang et al. (2012) all highlight the prominent reduction of SO_2 during 2007 and 2008, as a consequence of the widespread deployment of flue-gas desulfurization and the strict control strategy implemented for preparation of the 2008 Olympic Games. Throughout the past decade, 90% of the locations in China have shown a decline in SO_2 emissions, as highlighted by Koukouli et al. (2016). Such widespread declines are ascribed to effective air quality regulations enforced in China (van der A et al., 2017). Furthermore, Krotkov et al. (2016) and Li et al. (2017) both compared the sulfurous pollution in China and India, and pointed out their opposite trajectories. Since 2007, emissions in China have declined while those in India have increased substantially. Nowadays, India is overtaking China as the world's largest emitter of anthropogenic SO_2. In addition, several studies conducted analyses on SO_2 in sub-regions of China, for example Jin et al. (2016), Lin et al. (2012), Wang et al. (2015) and Su et al. (2011). All these studies contributed to a better understanding of SO_2 changes in China. However, there are still key issues to be addressed. First, with the pace of considerable progress made on SO_2 retrieval, updated data products are now available to accurately derive recent SO_2

© Author(s) 2018. CC BY 4.0 License.

variations in China. Second, although the general decreasing tendency has been revealed, the specific spatial and temporal regimes remain unclear. Does the SO_2 decrease monotonically, or is there a complicated oscillation? How similar/different are SO_2 variations in different parts of the country? Third, there is more to be learned about the driving mechanisms that govern SO_2 variations. Previous studies have mainly focused on the impact from amounts of emission. However, the SO_2 content is not only dependent on emissions but also on atmospheric conditions. Therefore, how large is the influence of atmospheric variability on the variation of SO_2?

The overall goal of this study is to quantify the spatial and temporal changes of SO_2 regimes over China in the last decade and to disclose the driving mechanism, based on a new-generation of SO_2 retrieval dataset (Theys et al., 2015). The manuscript is organized as follows. Section 2 describes the new SO_2 product, and statistical databases of SO_2 emission and atmospheric data are introduced. In Section 3, we evaluate the general patterns of SO_2 including mean distribution, long-term trends and seasonality. Subsequently, Section 4 identifies the specific regimes of SO_2 variability and the associated driving mechanisms. Finally, concluding remarks are presented in Section 5.

2 Data

The Ozone Monitoring Instrument (OMI) is one of four sensors onboard the Aura satellite launched in July 2004 (Levelt, J. et al., 2006). In recent years, Belgian Institute for Space Aeronomy has developed a new scheme to improve the retrieval accuracy of

© Author(s) 2018. CC BY 4.0 License.

SO_2 in troposphere. A new SO_2 product is generated based on the improved algorithm applied to OMI-measured radiance spectra (Theys et al. 2015). The retrieval scheme is a based on a DOAS approach, including three steps: (1) a spectral fit in the 312-326 nm range (other fitting windows are used for volcanic scenarios but are not relevant for this study), (2) a background correction for possible bias on retrieved SO_2 slant columns, (3) a conversion into SO_2 vertical columns through radiative transfer air mass factors calculation, accounting for the SO_2 profile shape (from the IMAGES chemistry transport model), geometry, surface reflectance and clouds. The dataset is made available on a 0.25° and 0.25° regular latitude-longitude grid over the rectangular domain 70-140°E, 10-60°N, and covers the period of 2005 to 2016 at monthly interval. In addition, a cloud screening is applied to remove measurements with a cloud fraction of more than 30%. Other details can be found in Theys et al. (2015).

The SO_2 emissions at national and provincial level are collected from the China Statistical Yearbook on Environment, which is compiled jointly by the National Bureau of Statistics, Ministry of Environmental Protection and other ministries. It is an annual statistics publication, with industrial and household emissions listed separately. Note that, in addition, the data for year 2016 are not available at present.

The large-scale meteorological conditions are taken from Japanese 55-year Reanalysis (JRA-55) data, prepared by the Japan Meteorological Agency (Kobayashi et al., 2015; Harada et al., 2016). The variables analyzed include total column precipitable water, horizontal wind and temperature at pressure levels.

© Author(s) 2018. CC BY 4.0 License.

3 General patterns of SO_2 over China

3.1 Mean distribution

Based on 12 years of SO_2 column data over China, Figure 1a shows the spatial pattern of long-term mean. Overall, SO_2 distribution is of great inhomogeneity in China, with two maximum centers: one is the North China Plain (NCP for short), and the other is Cheng-Yu (CY) district in Southwest China. In particular, SO_2 amount in NCP exceeds 1.2 DU. There are two essential causes responsible for high SO_2 loading in the two areas. On the one hand, combined effect of rapid economic and industrial development as well as population growth leads to a high degree of anthropogenic SO_2 emission. It is obvious in Figure 1b that the two regions release about 8.3 tons/km^2 SO_2 per year, which is three times greater than the average level of China. On the other hand, as shown in Figure 1c, either of the two regions is surrounded or partly surrounded by mountains, which makes it difficult for the pollutants to dissipate.

In contrast, over the sparsely populated western part of China, low SO_2 concentrations of less than 0.2 DU are observed, except over some provincial capitals. Since western part of China is less affected by human activities, anthropogenic sources of SO_2 are much smaller than natural emissions including emissions from terrestrial ecosystems and oxidation of H_2S to SO_2 (Wang et al., 1999). Between latitude 30-40°N, for example, the SO_2 amount over the eastern regions (110-120°E) are 6-12 times greater than western regions (80-110°E).

Atmos. Chem. Phys. Discuss., https://doi.org/10.5194/acp-2018-661
Manuscript under review for journal Atmos. Chem. Phys.
Discussion started: 24 July 2018
© Author(s) 2018. CC BY 4.0 License.

Atmospheric Chemistry and Physics
Discussions

Furthermore, the annual total is decomposed into seasonal cycle, as shown in Figure 2. In eastern China, nearly half of the annual totals is released in winter when intensive heating takes place, while SO_2 in summer only accounts for 10 percent. The remaining 40 percent is almost equally divided in spring and autumn. In western China, however, there is more SO_2 amounts in summer than other seasons, because large natural emissions occur in summer.

3.2 Long-term trends

Figure 3 depicts the spatial pattern of linear trends in annual and seasonal SO_2 from 2005 to 2016. Overall, apparent downward trends overwhelm most parts of eastern China, while western China has experienced little change. In particular, the most significant reduction occurred in the highly SO_2-polluted regions, with the decreasing rates amounting to 0.1 DU/a. This result suggests that the governments and communities in these economically developed regions have done its best to effectively control environmental pollution, including energy saving, emission cut and adjustment of energy consumption structure, shutdown of the most polluting factories, upgradation of coal quality, etc. Besides, enforcement of environmental protection laws is becoming more and more rigorous (van der A et al., 2017). Therefore, under collaborative efforts, the SO_2 levels in these highly developed regions with high background concentration have been decreasing markedly in the recent decade. Moreover, the pattern correlation between mean (Figure 1a) and trends (Figure 2 top) of SO_2 reaches to –0.77, implying that the downward rate over China can be summarized into a general rule—the higher

© Author(s) 2018. CC BY 4.0 License.

the SO_2 loading, the more significant the decrease.

Figure 2a-d portrays the long-term trends of SO_2 on seasonal basis. On the one hand, every season has witnessed SO_2 reduction, with the strongest decrease occurring in winter and autumn. Consequently, it can be concluded that the SO_2 decrease in winter and autumn contribute most to the reduction of annual SO_2. On the other hand, the highly SO_2-polluted regions have experienced the most pronounced decrease across all seasons, which is consistent with the annual outcomes.

3.3 Features of the four hotspots

Besides the NCP and CY regions with highest SO_2 loadings, this study is also interested in Yangtze River Delta (YRD) and Pearl River Delta (PRD), the other two economic mega-urban zones in China. These four identified hotspots NCP, CY, YRD and PRD are outlined in Figure 1a and will be specially examined in the following discussion.

In this part, we discuss the temporal behaviors of the four hotspots interested. Figure 4 depicts the SO_2 columns from 2005 to 2016 as a function of year (y-axis) and calendar month (x-axis). The horizontal axis is the month of the year, the vertical axis is the year, and the color is the SO_2 VCD for that month and year.

As regards seasonal cycle referenced to the x-axis on the bottom, the annual range of SO_2 rises progressively from south to north. NCP has the greatest amplitude of up to 1 DU, while there is virtually no annual cycle in PRD. Larger amplitude for SO_2 cycles in NCP arises from the reversed source-sink imbalance between summer and winter, in

© Author(s) 2018. CC BY 4.0 License.

the presence of intensive heating in winter and effective wet removal in summer. In contrast, the climate in PRD is characterized by smoother transition over the whole year and there is no heating season, which explains the insignificant seasonal variation of SO_2 in PRD. The other two regions CY and YRD have approximately the same amplitude of 0.6 DU, because they are on the same line of latitude. When looking at year-to-year variations on the vertical axis, SO_2 VCDs exhibit a decreasing tendency during the last decade, regardless of the time of the year.

4 Specific regimes of SO_2 variability and causes

4.1 Specific regimes of SO_2 variability

The above investigation presents SO_2 patterns and trends across China, but some elusive non-monotonic behaviors are not fully understood. In this section, we aim to detect the specific regimes of SO_2 variability and associated responsible mechanisms.

Spatiotemporal regimes of SO_2 over China are mapped by using empirical orthogonal function (EOF) decomposition (Hannachi, 2004), which is a useful tool to reduce the data dimensionality to two dimensions. One dimension represents the spatial structure and the other the temporal dimension. Figure 5 illustrates the leading mode (top) and the corresponding principal component (PC, bottom) obtained from EOF, since only the first mode is statistically well separated. Compared to the first EOF mode explaining 36.8% of the total variance, each of the other modes is characterized by less than 6% contribution and thus discarded. On the one side, the variation of SO_2 is

Atmos. Chem. Phys. Discuss., https://doi.org/10.5194/acp-2018-661
Manuscript under review for journal Atmos. Chem. Phys.
Discussion started: 24 July 2018
© Author(s) 2018. CC BY 4.0 License.

dominated by a spatially uniform feature with large loadings in NCP and CY, suggesting that SO_2 changes would be in the same phase but varying amplitude across the entire region. On the other side, the corresponding PC exhibit overall declines during the 2005 to 2016. However, the result does not implicate a simple continuous decrease. In fact, there appears to be a transient increase until a peak and thereafter two sharp drops occur in the periods 2007-2008 and 2014-2016, amid which SO_2 concentrations are under the process of slightly rebounding or stagnation. In short, the SO_2 variability is characterized by four distinct temporal regimes.

Moreover, Figure 6 demonstrates the time series for each hotspot with linear regression lines over the entire timespan and four sequential segments added. The green fitting lines reveal that SO_2 in NCP, CY, YRD and PRD had undergone an overall downward trend with a rate of 0.062, 0.059, 0.046 and 0.055 DU per year, respectively. However, the SO_2 decrease is not monotonic, but varied in four stages: a short-lived increasing period at the beginning, a steep drop period during 2007 to 2008, a continued stagnation or slowly rebound period of 2009 to 2013 and another drastic drop period during 2014 to 2016. Note that only PRD had experienced a persistent decrease in SO_2 since 2007.

Figure 7a depicts the temporal structure classification of SO_2 VCD for each province, with red color implying non-monotonic decrease whereas linearly decline is colored by green. Northeast China and Western China are excluded from the analysis, due to lots of missing data during winter in the former domain and extremely low concentrations

© Author(s) 2018. CC BY 4.0 License.

in the latter one. From the map, it is clear that over most of China except Guangdong and Guizhou provinces, SO_2 does not evolve in a monotonic way but shows either a rebound or stagnation during 2009 to 2013.

4.2 Causes

In this section, we diagnose the likely mechanisms behind the observed SO_2 variability. Generally, emissions and meteorological conditions are two main factors that essentially exert influence on atmospheric pollutant load. Despite spatially uniformity in temporal-pattern classification of SO_2 VCD (Figure 7a), temporal structure of emission demonstrates strong south-north contrast (Figure 7b). Thus, it is advantageous to divide the Eastern China into north part and south part to examine the causes. To this end, North China and South China are treated separately. Figure 8 presents time series and scatter plots of SO_2 VCD and emission, and Figure 9 is designed to show the total emission generated by industries and households.

As shown in Figure 8a, the North China features a good correspondence between amount and emission, with linear correlation of 0.9. Time series of emission also indicate the existence of four distinct regimes that are likely to drive the regime of SO_2 VCD directly. This is confirmed by the scatter plot (Figure 8b), in which the points are tightly clustered around the regression line. Based on variance analysis, emission accounts for 81% fraction of SO_2 VCD variation over North China. Furthermore, as shown in Figure 9a, the industrial emissions play a crucial role in SO_2 VCD variation throughout the whole period in North China, while household emissions fluctuate little

© Author(s) 2018. CC BY 4.0 License.

until 2008. However afterwards it acts to partially offset the effect caused by industrial emissions.

The close linear relationship observed in North China is not found in South China, since the two curves appear to become no adherent in Figure 8c and the points in the scatter plot Figure 8d are widely spread around the regression line. Variance analysis suggests that only 36% of SO_2 VCD variability is forced by emissions, suggesting that the SO_2 variations in South China cannot be explained by emission changes alone. This is mainly ascribed to the decoupled pathways of emission and SO_2 VCD during 2009 to 2013, as the emission continues to decline but SO_2 VCD witnesses a rebound. Figure 9b suggests that the gradual cut of industrial emissions together with a sudden shift of emissions in household sector collectively promote the continuous decrease of total emission in South China, which is different from that in North China.

Why decreasing emissions do not cause a reduction of SO_2 VCD in South China during 2009 to 2013? To answer this question, the atmospheric conditions during 2009 to 2013 are compared with those during the rest of the years, as depicted in Figure 10. The period 2009 to 2013 is characterized by prolonged dry conditions in South China with the precipitable water and precipitation being lower than usual (Figure 10a), which weakens wet adsorption and scavenging. At the same time, this period is also associated with relatively weaker wind speed (Figure 10b) and increased static stability (Figure 10c, d), reducing the ability of the atmosphere to diffuse leading to the accumulation of SO_2 loads. In brief, unfavorable meteorological conditions produce the observed

Atmos. Chem. Phys. Discuss., https://doi.org/10.5194/acp-2018-661
Manuscript under review for journal Atmos. Chem. Phys.
Discussion started: 24 July 2018
© Author(s) 2018. CC BY 4.0 License.

rebound of SO_2 during 2009 to 2013, despite the continued decrease of emission.

5 Conclusions

In this study, the spatiotemporal variability of SO_2 columns over China and the associated driving mechanisms are examined over the past decade. Based on a state-of-the-art SO_2 retrieval dataset recently derived from the OMI instrument, we produce an improved database suitable for the study of SO_2 changes in China and we elaborate on the specific SO_2 regimes and underlying causes.

Climatological SO_2 in China has an uneven spatial distribution in space and time. East China is far more exposed to SO_2 pollution than West China, with two maxima centered in NCP and CY. From analysis of the annual cycles we conclude that half of the annual totals are released in winter, while SO_2 in summer only accounts for 10 percent. In addition, the annual amplitude of SO_2 rises progressively from south to north.

From 2005 through 2016, most of eastern China presents a clear decreasing tendency for SO_2, while western China has experienced little change. Spatially, the decreasing rate is generally enhanced for high SO_2 loads. When computed seasonally, SO_2 reductions in winter and autumn contribute most to the reduction of annual SO_2.

Four stages of variation are identified by EOF analysis. The first regime (2005-2006) features a transient increasing trend, the second (2007-2008) and the last (2014-2016) regimes show sharp drops, and the third regime (2009-2013) manifests itself by 5-year moderate rebounding or continued stagnation. Although temporal regimes of SO_2 are

© Author(s) 2018. CC BY 4.0 License.

coherent throughout the country, different driving forces are tied to North China and South China delimited roughly by the Yangtze River. In North China, the atmospheric SO_2 and emission varies essentially in the same way. Therefore, the atmospheric SO_2 variability is primarily associated with the emission variability, which accounts for 81% of the total variance. Further, the emission generated by industrial sector is largely responsible for the atmospheric SO_2 variability. The household emissions appears to remain stable until 2008, but afterwards they act to partially offset the impact of industrial emissions.

SO_2 emissions in South China exhibit a continuous decreasing tendency, due to the gradual cuts of industrial emissions together with a sudden downward shift of household emissions. As a result, the role of emissions only contributes one third of the SO_2 variation, primarily owing to the decoupled pathways of emission and atmospheric content during 2009 to 2013 when the emission continues to decline but atmospheric content witnesses a rebound. It is found that such rebound occurs in response to the joint effect of deficient precipitation, weaker wind speed and increased static stability during 2009-2013.

Acknowledgement: This work was supported by the National Key Research and Development Program of China nos. 2017YFB0504000 and 2016YFC0200403, and the National Natural Science Foundation of China nos. 41505021 and 41575034.

Atmos. Chem. Phys. Discuss., https://doi.org/10.5194/acp-2018-661
Manuscript under review for journal Atmos. Chem. Phys.
Discussion started: 24 July 2018
© Author(s) 2018. CC BY 4.0 License.

6 References

Chai, F., Gao, J., Chen, Z., Wang, S., Zhang, Y., Zhang, J., Zhang, H., Yun, Y., and Ren, C.: Spatial and temporal variation of particulate matter and gaseous pollutants in 26 cities in China, Journal of Environmental Sciences, 26(1), 75-82, 2014.

Chan, C. K., and Yao, X.: Air pollution in mega cities in China, Atmospheric Environment, 42(1), 1-42, 2008.

Hannachi, A.: A primer for EOF analysis of climate data. Reading: University of Reading, 2004.

Harada, Y., and Coauthors: The JRA-55 Reanalysis: Representation of atmospheric circulation and climate variability, Journal of the Meteorological Society of Japan. Ser. II, 94(3), 269-302, 2016.

Jin, J., Ma, J., Lin, W., Zhao, H., Shaiganfar, R., Beirle, S., and Wagner, T.: MAX-DOAS measurements and satellite validation of tropospheric NO2 and SO2 vertical column densities at a rural site of North China, Atmospheric Environment, 133, 12-25, 2016.

Kobayashi, S., and Coauthors: The JRA-55 reanalysis: General specifications and basic characteristics, Journal of the Meteorological Society of Japan. Ser. II, 93(1), 5-48, 2015.

Koukouli, M. E., and Coauthors: Anthropogenic sulphur dioxide load over China as observed from different satellite sensors, Atmospheric Environment, 145, 45-59,

© Author(s) 2018. CC BY 4.0 License.

2016.

Krotkov, N. A., and Coauthors: Aura OMI observations of regional SO_2 and NO_2 pollution changes from 2005 to 2015, Atmospheric Chemistry and Physics, 16(7), 4605-4629, 2016.

Lee, C., and Coauthors: SO_2 emissions and lifetimes: Estimates from inverse modeling using in situ and global, space‐based (SCIAMACHY and OMI) observations, Journal of Geophysical Research: Atmospheres, 116(D6), 2011.

Levelt, P. F., and Coauthors: The ozone monitoring instrument, IEEE Transactions on Geoscience and Remote Sensing, 44(5), 1093-1101, 2006.

Li, C., Zhang, Q., Krotkov, N. A., Streets, D. G., He, K., Tsay, S. C., and Gleason, J. F.: Recent large reduction in sulfur dioxide emissions from Chinese power plants observed by the Ozone Monitoring Instrument, Geophysical Research Letters, 37(8), 2010.

Li, C., Joiner, J., Krotkov, N. A., and Bhartia, P. K.: A fast and sensitive new satellite SO2 retrieval algorithm based on principal component analysis: Application to the ozone monitoring instrument. Geophysical Research Letters, 40(23), 6314-6318, 2013.

Li, C., and Coauthors: India is overtaking China as the world's largest emitter of anthropogenic sulfur dioxide, Scientific Reports, 7(1), 14304, 2017.

Lin, W., Xu, X., Ma, Z., Zhao, H., Liu, X., and Wang, Y.: Characteristics and recent trends of sulfur dioxide at urban, rural, and background sites in North China:

© Author(s) 2018. CC BY 4.0 License.

Effectiveness of control measures, Journal of Environmental Sciences, 24(1), 34-49, 2012.

Lu, Z., and Coauthors: Sulfur dioxide emissions in China and sulfur trends in East Asia since 2000, Atmospheric Chemistry and Physics, 10(13), 6311-6331, 2010.

Ma, J., Xu, X., Zhao, C., and Yan, P.: A review of atmospheric chemistry research in China: Photochemical smog, haze pollution, and gas-aerosol interactions. Advances in Atmospheric Sciences, 29(5), 1006-1026, 2012.

Meng, X. Y., Wang, P. C., Wang, G. C., Yu, H., and Zong, X. M.: Variation and transportation characteristics of SO2 in winter over Beijing and its surrounding areas, Climatic and Environmental Research, 14(3), 309-317, 2009. (in Chinese)

MEPC (Ministry of Environmental Protection of China): Technical regulations on ambient air quality index (on trial), 2012.

Munro, R., and Coauthors: GOME-2 on MetOp, Proc. of The 2006 EUMETSAT Meteorological Satellite Conference, Helsinki, Finland, 1216, 48, 2006.

Ren, L., Yang, W., and Bai, Z.: Characteristics of Major Air Pollutants in China, in Ambient Air Pollution and Health Impact in China, Springer, 7-26, 2017.

Rix, M., and Coauthors: Volcanic SO2, BrO and plume height estimations using GOME‐2 satellite measurements during the eruption of Eyjafjallajökull in May 2010, Journal of Geophysical Research: Atmospheres, 117(D20), 2012.

Su, S., Li, B., Cui, S., and Tao, S.: Sulfur dioxide emissions from combustion in China: from 1990 to 2007, Environmental Science and Technology, 45(19), 8403-8410,

© Author(s) 2018. CC BY 4.0 License.

2011.

Theys, N., and Coauthors: Sulfur dioxide vertical column DOAS retrievals from the Ozone Monitoring Instrument: Global observations and comparison to ground - based and satellite data, Journal of Geophysical Research: Atmospheres, 120(6), 2470-2491, 2015.

van der A, R. J., Mijling, B., Ding, J., Koukouli, M. E., Liu, F., Li, Q., Mao, H., and Theys, N.: Cleaning up the air: effectiveness of air quality policy for SO2 and NOx emissions in China, Atmos. Chem. Phys., 17, 1775-1789, 2017.

Wang, M: Atmospheric Chemistry (second edition), China Meteorological Press, 1999. (in Chinese).

Wang, S., and Coauthors: Satellite measurements oversee China's sulfur dioxide emission reductions from coal-fired power plants, Environmental Research Letters, 10(11), 114015, 2015.

Wang, T., Hendrick, F., Wang, P., Tang, G., Clémer, K., Yu, H., Fayt, C., Hermans, C., Gielen, C., Müller, J.-F., Pinardi, G., Theys, N., Brenot, H., and Van Roozendael, M.: Evaluation of tropospheric SO2 retrieved from MAX-DOAS measurements in Xianghe, China, Atmos. Chem. Phys., 14, 11149-11164, 2014.

WHO (World Health Organization): Ambient (outdoor) air quality and health, 2018, http://www.who.int/news-room/fact-sheets/detail/ambient-(outdoor)-air-quality-and-health.

Yan, H., Chen, L., Su, L., Tao, J., and Yu, C.: SO_2 columns over China: Temporal and

© Author(s) 2018. CC BY 4.0 License.

spatial variations using OMI and GOME-2 observations, IOP Conference Series: Earth and Environmental Science, 17(1), 012027, 2014.

Yu, H., Wang, P., Zong, X., Li, X., and Lü, D.: Change of NO_2 column density over Beijing from satellite measurement during the Beijing 2008 Olympic Games, Chinese Science Bulletin, 55(3), 308-313, 2010.

Zhang, X., van Geffen, J., Liao, H., Zhang, P., and Lou, S.: Spatiotemporal variations of tropospheric SO2 over China by SCIAMACHY observations during 2004–2009, Atmospheric Environment, 60, 238-246, 2012.

Zhang, Y., Li, C., Krotkov, N. A., Joiner, J., Fioletov, V., and McLinden, C.: Continuation of long-term global SO2 pollution monitoring from OMI to OMPS. Atmospheric Measurement Techniques, 10(4), 1495-1509, 2017.

© Author(s) 2018. CC BY 4.0 License.

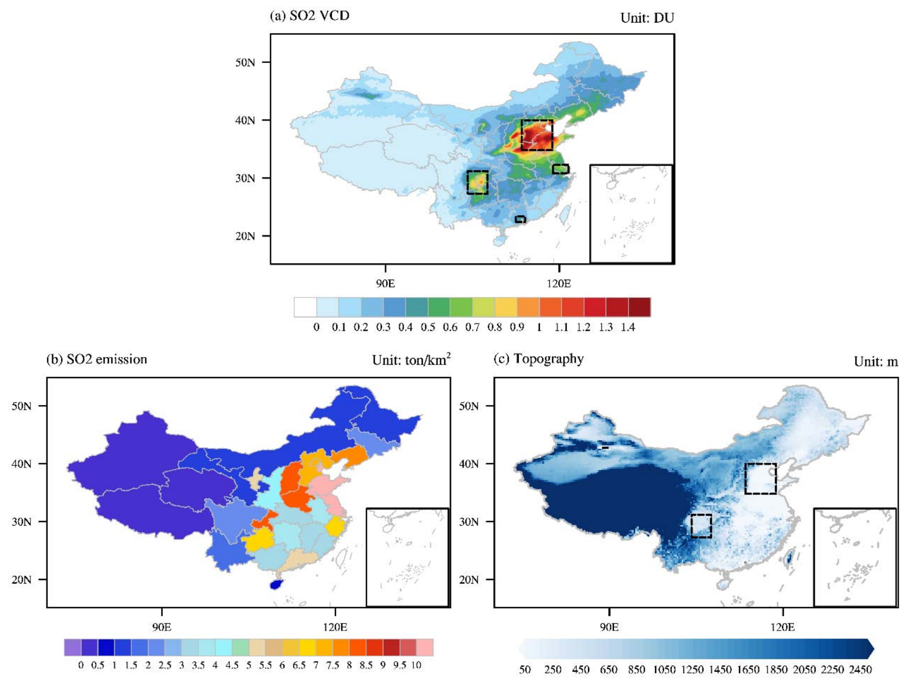

Figure 1 (a) Spatial distribution of 12-year (2005–16) averaged tropospheric SO2 Vertical Column Density (VCD) over China. (b) SO_2 emission per km^2 among Chinese provinces. (c) Topography of China in meters.

© Author(s) 2018. CC BY 4.0 License.

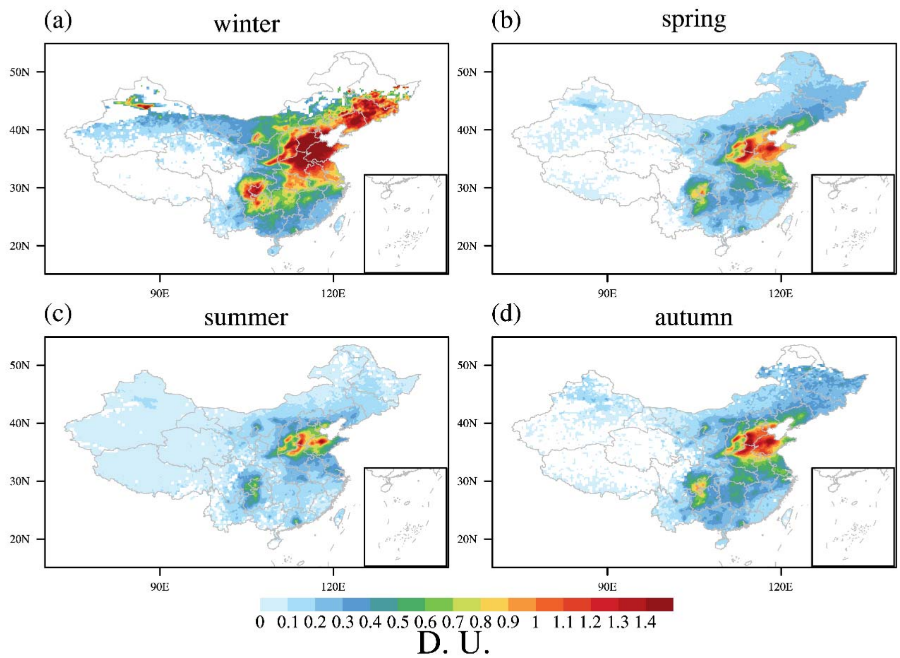

430

431 Figure 2 Seasonal tropospheric SO2 over China: (a) winter, (b) spring, (c) summer and (d) autumn

432

433

© Author(s) 2018. CC BY 4.0 License.

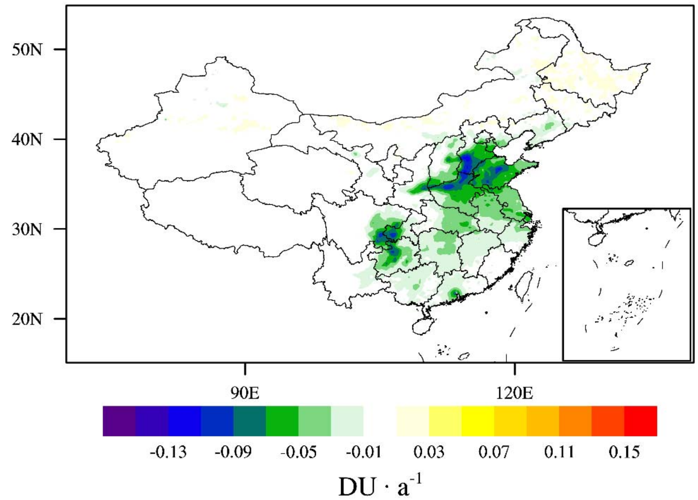

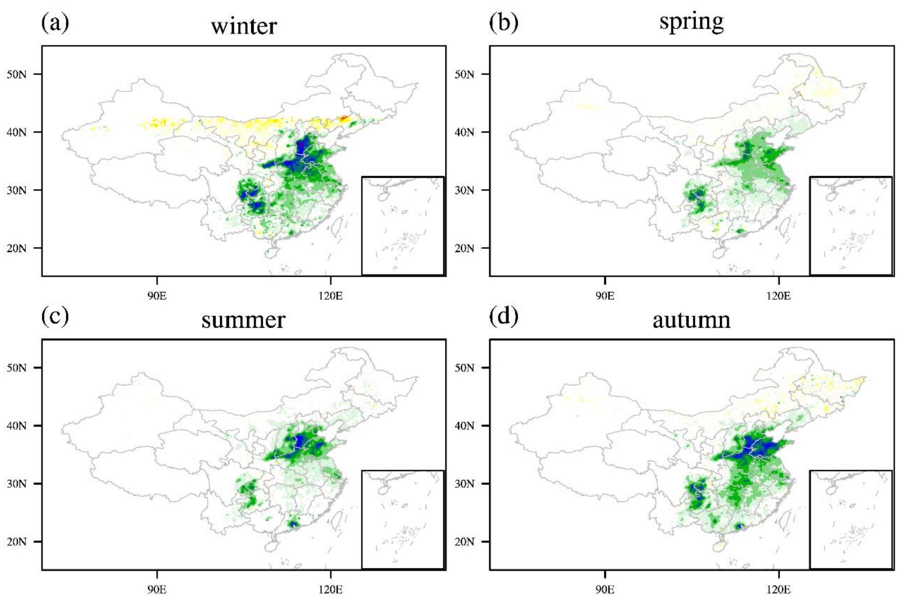

Figure 3 Spatial pattern of SO_2 linear trends (2005–16) in annual (Top) and seasonal values (a, b, c, d)

Atmos. Chem. Phys. Discuss., https://doi.org/10.5194/acp-2018-661
Manuscript under review for journal Atmos. Chem. Phys.
Discussion started: 24 July 2018
© Author(s) 2018. CC BY 4.0 License.

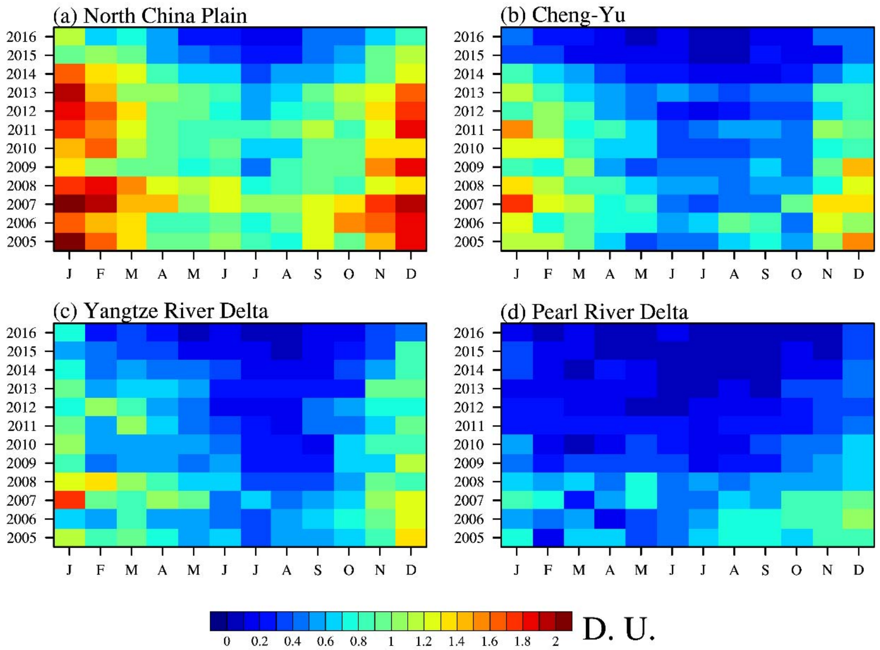

Figure 4 SO_2 amounts from 2005 to 2016 as a function of year (y-axis) and calendar month (x-axis) for NCP (a), CY (b), YRD (c) and PRD (d).

© Author(s) 2018. CC BY 4.0 License.

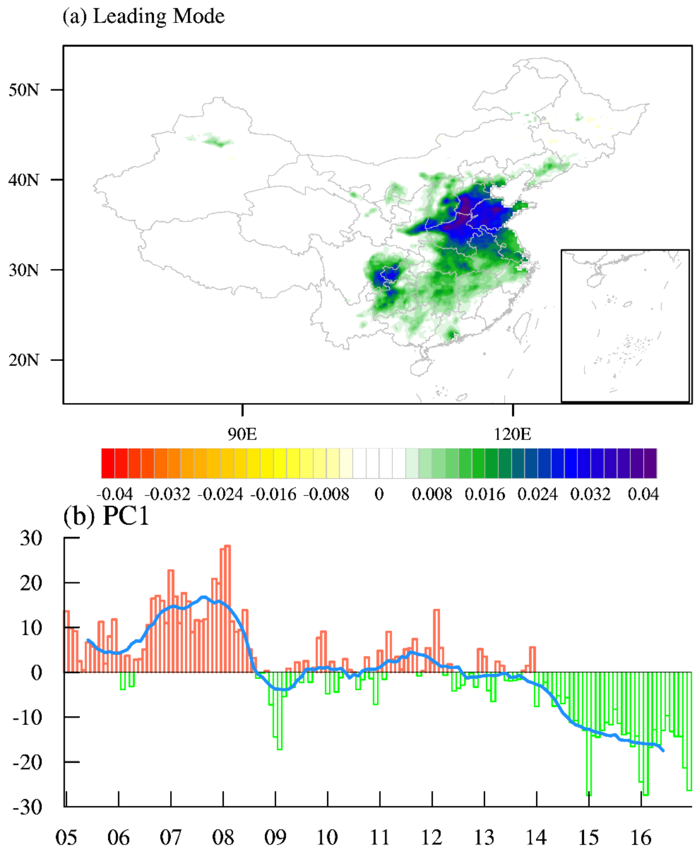

Figure 5 The first leading EOF mode (a) and the corresponding principal components (b)

© Author(s) 2018. CC BY 4.0 License.

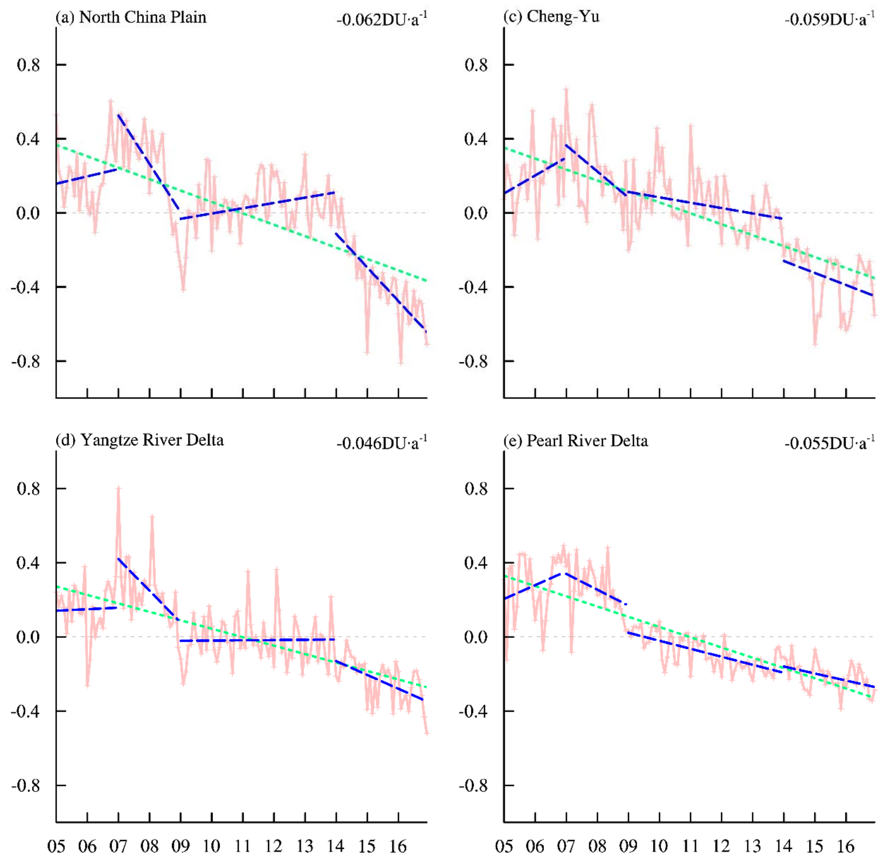

Figure 6 Temporal evolution of SO_2 anomalies over four hotspots (a, b, c, d), with slope lines over the entire timespan (green) and four sequential segments (blue) superimposed

© Author(s) 2018. CC BY 4.0 License.

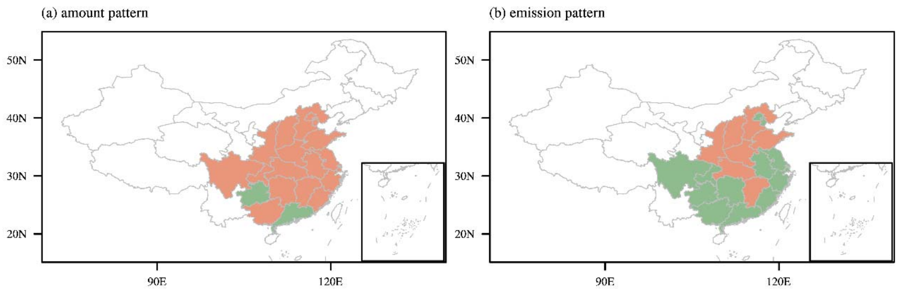

Figure 7 Temporal structure classification of SO_2 VCD (a) and emission (b). Red color implies non-monotonic decrease with either a rebound or stagnation in the middle, while monotonic decrease is colored by green.

Atmos. Chem. Phys. Discuss., https://doi.org/10.5194/acp-2018-661
Manuscript under review for journal Atmos. Chem. Phys.
Discussion started: 24 July 2018
© Author(s) 2018. CC BY 4.0 License.

Atmospheric Chemistry and Physics
Discussions
Open Access

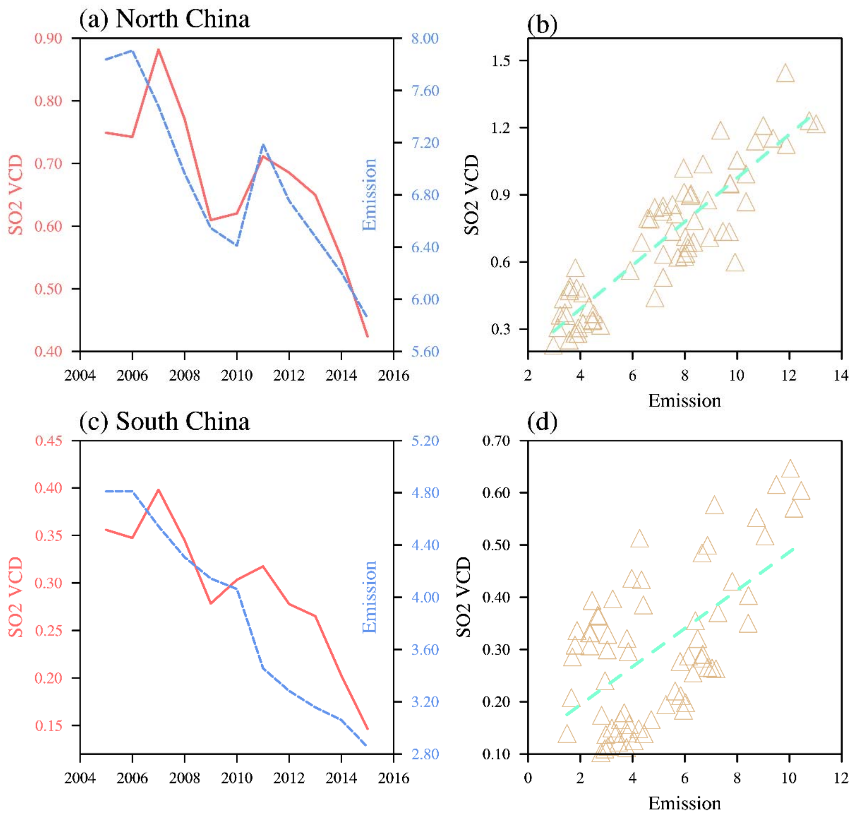

Figure 8 Time series plots of SO2 VCD and emission (a, c), and scatter plots with regression line of SO2 VCD and emission (b, d) for North China (1st Row) and South China (2nd Row)

© Author(s) 2018. CC BY 4.0 License.

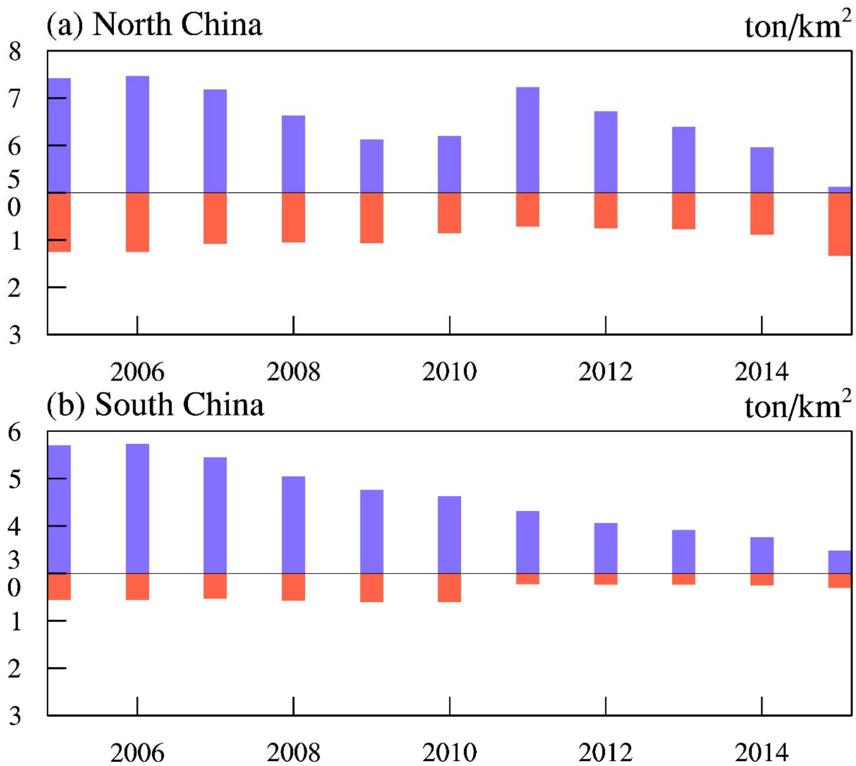

Figure 9 Annual SO2 emission (ton/km^2) generated by industries (upward blue bars) and households (downward red bars) in North China (a) and South China (b). Notice that the Y-axis in a positive direction does not start at zero.

Atmos. Chem. Phys. Discuss., https://doi.org/10.5194/acp-2018-661
Manuscript under review for journal Atmos. Chem. Phys.
Discussion started: 24 July 2018
© Author(s) 2018. CC BY 4.0 License.

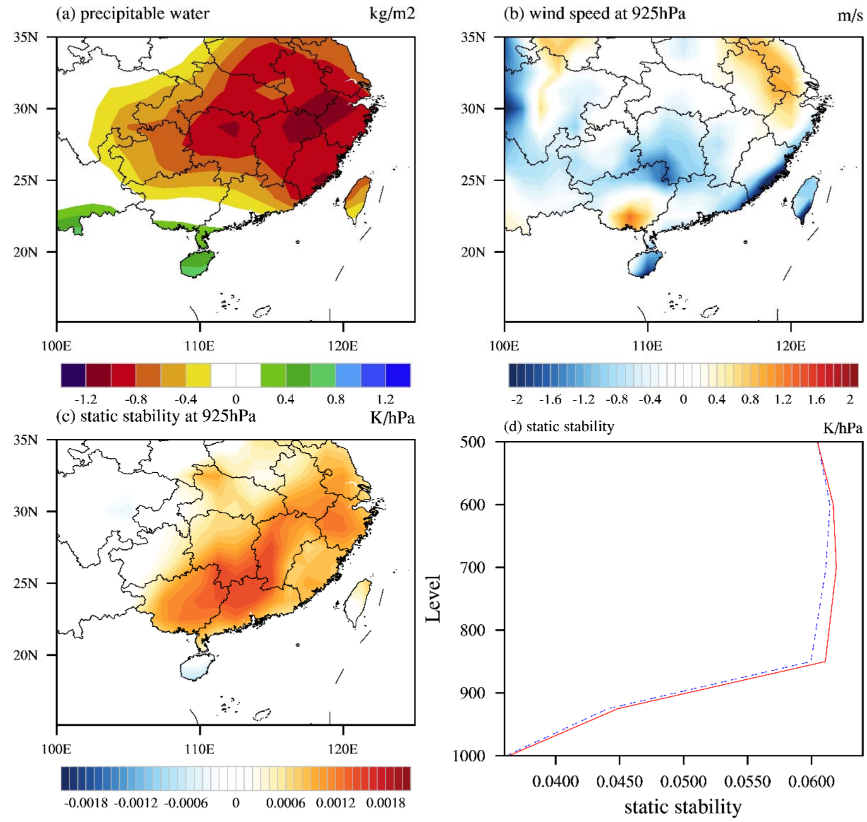

Figure 10 Comparison of atmospheric conditions between the period of 2009-2013 and the other years: (a) composite difference in precipitable water (unit: kg/m^2), (b) composite difference in wind velocity at 925hPa (unit: m/s), (c) composite difference in static stability at 925hPa (unit: K/hPa), and (d) averaged vertical profile of static stability for the two episodes.